*energies*

MDPI

*Article*

# Magnetic Vibration in Induction Motor Caused by Supply Voltage Distortion

**Artem Ermolaev [1], Vladimir Erofeev [1], Aleksandr Plekhov [2] and Dmitry Titov [2,*]**

[1] The Mechanical Engineering Research Institute of the Russian Academy of Sciences, 603024 Nizhny Novgorod, Russia
[2] Department of Electric Power Engineering, Power Supply and Power Electronics, Nizhny Novgorod State Technical University n.a. R.E. Alekseev, 603950 Nizhny Novgorod, Russia
* Correspondence: d.titov@nntu.ru

**Abstract:** This article discusses magnetic vibrations in squirrel-cage induction motor stators and provides a mathematical description of the process of their excitation. A model of a 30 kW squirrel-cage induction motor was developed in finite element software. This model considers the motor geometry, material properties and stator winding. The electromagnetic and mechanical processes in the motor during the rotation of the rotor were considered. In the course of this study, currents of various harmonic compositions and amplitudes were applied to the motor windings, which caused magnetic noise, vibration and pulsations of the electromagnetic torque. Magnetic noises, vibrations and pulsations of the electromagnetic torque were investigated in the case of imbalance and harmonic distortions of the supply voltage.

**Keywords:** squirrel-cage induction motor; magnetic vibrations; radial magnetic forces; Maxwell forces; finite element method; voltage distortion; voltage unbalance; stator deformations



**Citation:** Ermolaev, A.; Erofeev, V.; Plekhov, A.; Titov, D. Magnetic Vibration in Induction Motor Caused by Supply Voltage Distortion. *Energies* **2022**, *15*, 9600. https://doi.org/10.3390/en15249600

Academic Editor: Andrea Mariscotti

Received: 17 November 2022
Accepted: 15 December 2022
Published: 17 December 2022



## 1. Introduction

Magnetic vibration is a problem for almost all medium- and high-power electric motors [1–5]. It causes adverse events: a change in the harmonic composition of the supply current [6,7], bearing wear [8], acoustic noise [9,10], an increase in power consumption [11,12] and the destruction of electric motors [13,14]. This problem occurs in the electric drive [15,16] and generators, including wind turbines [17,18].

The most strongly magnetic vibration is manifested in asynchronous squirrel-cage induction motors (SCIM), characterized by a rotating magnetic field relative to the stationary stator of the machine. Waves of radial magnetic force cause periodic deformations of the stators of motors, which manifests primarily in the form of acoustic noise.

Much research from has been devoted to the study of magnetic vibration and the development of methods to suppress it. In the 1970–1980s, research provided a fundamental base for the mathematical description of magnetic vibrations of electrical machines and the structural methods for their reduction [19,20]. In the 1990–2000s, researched methods focused on actively reducing the magnetic vibration occurring in the SCIM stator. These methods are based on adding a compensation harmonic to the supply voltage [4,21–23]. Completely different approaches were offered by the methods proposed in the works of the last decade [1,24,25]. In these works, the control of magnetic vibration is achieved by a given change in angles of voltages in the vector control system of an SCIM-based electric drive.

Almost all known methods of reducing magnetic vibrations in SCIM are based on the same theoretical base, within which magnetic fields, radial magnetic forces (Maxwell forces) and stator deformations are waves of a certain frequency, spatial order (mode number) and amplitude. At the same time, the reduction in magnetic vibration is achieved through effective control of the parameters of the motor supply voltage, for which it is necessary to

know the relationship of these physical quantities. The task of analytical representation of this relationship is complicated by numerous irregularities and assumptions that cannot be taken into account due to the complex and time-varying geometry of an investigated motor. Therefore, it is advisable to carry out interconnected mechanical, acoustic, and electromagnetic calculations of processes occurring in a motor under operation with finite-element multiphysics design software.

The study is applicable to alternating current motors of medium and high power, from 15 to 150 kW, and with a speed of 1500–3000 rpm. These machines do not have a bevel groove in the rotor, and the air gap reaches 0.5–0.8 mm. Magnetic vibrations are much weaker in low-power motors due to the bevel groove and lower magnetic flux density. Bearing vibration and rotor eccentricity exceed magnetic vibration in such motors. In high-power alternating-current motors, magnetic vibrations are also a serious problem. They are a powerful source of noise. In any alternating current motors, the magnetic vibration is 5–10 times greater than in direct-current machines.

This article is a logical continuation of the work [26,27] devoted to the development of an FEM model of the AIR180M4U3 motor and the study of electromagnetic and mechano-acoustic processes. The method of active reduction of magnetic noise is described in [26]. The method is based on the injection of an additional compensation current of the electric motor to reduce the harmonics of the magnetic field. The developed method reduces the radial magnetic force by 20%, the harmonics of the magnetic force by 70%, and the amplitude of the stator displacement oscillations by 30%. The article [27] describes magnetic forces, mechanical stress fields, sound pressure and stator oscillation modes at sinusoidal voltage.

The purpose of this article is to study the mechano-acoustic processes in this motor when the shape of the supply voltage is distorted due to voltage imbalance and high harmonic distortion.

## 2. Magnetic Vibration Excitation in SCIM Stator

Waves of radial magnetic forces in defect-free SCIMs, which are the main sources of their vibration [20,26], are caused by the action of the magnetic field $B$ in the air gap on the stator steel [20]:

$$F_r(x,t) = \frac{B^2(x,t)}{2 \cdot \mu_0}, \quad (1)$$

where $\mu_0$—vacuum permeability, $t$—time, and $x$—angular coordinate of air gap (rad.).

One of the ways to reduce the vibrations of SCIM is to control the spectral composition of the magnetic field in the air gap [28]. The most common method involves active reduction of SCIM vibrations based on stator voltage control. In this case, an additional compensation harmonic or several harmonics generated by PWM are added to the fundamental supply voltage component. The task of the compensation harmonic is to suppress one of the harmonics of the magnetic field generated by the supply voltage, which causes the most intense vibrations of the SCIM stator. A detailed description of the essence and implementation of this method is described in [21,22].

The radial magnetic force generated by the magnetic field in the air gap of the SCIM is powered by the PWM inverter:

$$F_r(x,t) = \frac{1}{2\mu_0}\left(B_1(x,t) + B^i(x,t) + \sum_{g=2}^{\infty} B_g(x,t)\right)^2, \quad (2)$$

where $g$—magnetic field harmonic number, $B_1(x,t)$—first magnetic field harmonic, $B^i(x,t)$—$i$th magnetic field harmonic caused by injected current, and $B_g(x,t)$—higher-order harmonic of the magnetic field due to stator and rotor slots, air gap unevenness, etc.

The injected current should have small amplitude values (no more than 15% of the supply current amplitude for the 3rd harmonic and even less for the others [21]). In this case, the amplitudes of the radial magnetic forces, determined by the values of the magnetic

field in the air gap with the values $(B_m{}^i)^2/4\mu_0$ and $B_m{}^i \cdot \Sigma B_{mg}/2\cdot\mu_0$, will be negligible (the "$m$" index means the peak value). $THD_F$ in this case will change by no more than 19.3% (in the case of injection of 3, 5, 7, 11 and 13 harmonics with amplitudes of 0.15%, 0.9%, 0.7% 0.4% and 0.3% of the amplitude of the main harmonic of the supply voltage, respectively). Only two harmonics of the radial magnetic force generated by the interaction of the first magnetic field harmonic and the compensatory harmonic have a significant effect. These harmonics are described by the following equation:

$$F_r^i(x,t) = \frac{B_m^i \cdot B_{m1}}{2\mu_0} \cdot \left(\cos\left[2\cdot Z_p \cdot x - (\omega^i + \omega_1)\cdot t - (\varphi^i + \varphi_1)\right] + \cos\left[-(\omega^i - \omega_1)\cdot t - (\varphi^i - \varphi_1)\right]\right), \quad (3)$$

where $B_{m1}$—first magnetic flux density harmonic amplitude, $B_{mg}$—$g$th magnetic flux density harmonic amplitude, $B_m^i$—compensating harmonic amplitude, $Z_p$—pair of poles number, $\omega_1$—magnetic field angular frequency, $\varphi_1$—phase shift of first magnetic field harmonic, $\omega^i$—magnetic field angular frequency of injected harmonic, and $\varphi^i$—phase shift of injected harmonic.

These harmonics of radial magnetic force have a mode number of $2\cdot Z_p$ and 0.

It is necessary to know the basic parameters (angular frequency, amplitude and phase shift) in order to determine the most pronounced harmonics of the magnetic force:

$$F_r(x,t) = F_m \cdot \cos(r\cdot x - \omega\cdot t - \varphi), \quad (4)$$

where $F_m$—radial magnetic force amplitude, $r$—mode number, $\omega$—angular frequency of magnetic force ($\omega \approx 2\omega_1$), and $\varphi$—phase shift of magnetic force.

The harmonic with the mode number $r = 0$ according to [20] remains and will cause vibrations; however, its amplitude will be much smaller compared to the force Equation (4).

The mode number $r = 0$ causes uniform radial deformation of the stator along the entire air gap, radial magnetic forces of the second mode number ($r = 2$) and higher cause bending deformations of the stator, as shown in Figure 1 [20].

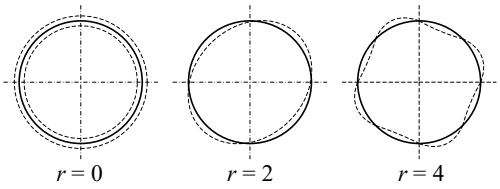


**Figure 1.** Deformation shapes of the stator.

## 3. Calculation of Magnetic Vibration Occurring in SCIM Stator

The radial magnetic forces of one harmonic composition cause vibrations in the SCIM stator of another harmonic composition. This is due to the fact that the SCIM stator is characterized by its own frequency response with one or several eigenfrequencies. Consequently, due to the resonant amplification, the spectral composition of the radial magnetic forces will be strikingly different from the harmonic composition of the stator vibrations.

With a mode number of $r = 2$ and above, the stator undergoes deformations of a complex spatial shape of an $r$-gon with an eigen angular frequency equal to [20].

$$\omega_r = \frac{r(r^2-1)}{\sqrt{r^2+1}} \sqrt{\frac{E\cdot h^3}{12\cdot m\cdot R_{st}^4}}, \quad (5)$$

where $E$—the elastic modulus of the stator, $h$ is the height of the stator back, $R_{st}$—the stator radius, and $m$—the reduced mass of the stator yoke determined by

$$m = \frac{m_{st}}{2\pi R_{st} l_{st}}, \quad (6)$$

where $m_{st}$—the mass of the stator core and $l_{st}$—the length of the stator.

Analysis of Equation (5) allows us to conclude that vibrations with the mode number of $r = 2$ are characterized by the highest intensity, since their frequency is lower than that of other ones [20]. At the same time, vibrations also have a significant effect on the stator magnetic noise in the case of the SCIM power supply from the PWM inverter. The mode number of these vibrations is $r = 2 \cdot Z_p = 4$.

The mechanical impedance $z_\omega$ of the SCIM stator at the angular frequency $\omega$ of the radial magnetic force is determined as follows:

$$z_\omega = \omega m - \frac{1}{\omega \lambda_{st}} = \omega m - \frac{Eh}{R_{st}^2 \omega}, \tag{7}$$

where $\lambda_{st}$—mechanical flexibility.

Vibrations arise due to the interaction of the first and higher harmonics of the magnetic field in the air gap of the SCIM. Waves of radial magnetic forces can be expressed on condition as follows (on condition $\omega_0 \rightarrow \omega_1$):

$$F_r(x,t) = \sum_{g=1}^{\infty} F_{rgm} \cos\left((Z_p \pm Z_p)x - 2(1 \pm g)\omega_1 t - (\varphi_{12} \pm \varphi_{12g})\right), \tag{8}$$

where $F_{rgm}$—amplitude value of magnetic force harmonic:

$$F_{rgm} = \frac{B_\delta^2 R I_{12g}}{2\mu_0 R_{st} I_{12}}, \tag{9}$$

where $B_\delta$—root mean square amplitude of magnetic flux density in the air gap, $R$—inner radius of the stator, $I_{12g}$ and $\varphi_{12g}$—amplitude and phase shift of the $g$th harmonic of magnetizing current, $I_{12}$ and $\varphi_{12}$—amplitude and phase shift of the first harmonic of magnetizing current.

## 4. Multiphysics FEM model of SCIM

The theory presented in the previous section allows us to accurately describe the processes of magnetic vibration excitation in the SCIM stators. However, it contains a large number of assumptions and restrictions regarding the shape of the air gap, changes in the geometry of the engine due to rotation of the rotor and deformation of the stator, and the shape and harmonic composition of the supply voltage on the stator windings. Accounting for each of these factors leads to a significant complication of mathematical expressions describing the processes of magnetic vibration excitation and often requires the introduction of additional restrictions, for example, taking into account only two or three harmonics of the supply current when describing magnetic induction waves or taking into account stator and rotor slots [20]. If magnetic induction waves are described using the harmonic conductivities method, then an assumption appears in the equation that the width of the air gap is constant in time when calculating the magnetic conductivity function [24].

In [26], a model of SCIM of an investigated motor with a power of 30 kW and synchronous rotation speed of 1500 rpm, developed in the multiphysics FEM design software, was presented. The motor under investigation was classified as medium power (20–250 kW). Therefore, the waves of radial magnetic force acting on the stator have a mode number of $r = 4$. Some geometric and technical characteristics of the motor are given in Table 1.

The number of rotor slots was reduced from 39 to 36 to simplify the model and increase the convergence of calculations. The stator winding in each slot is represented by a separate homogeneous multiturn coil. The other end of this coil closes outside the stator. The rotor winding is represented by a solid copper conductor, which is a squirrel cage. The geometry of the SCIM model of the investigated motor and the mesh are shown in Figure 2a,b.

**Table 1.** Type 30 kW induction motor parameters.

| Parameter | Value | Unit |
|---|---|---|
| Rated voltage | 380 | V |
| Rated current | 57 | A |
| Rated power | 30 | kW |
| Frequency | 50 | Hz |
| Number of pole pairs | 2 | – |
| Stator core outer diameter | 0.313 | m |
| Stator core inner diameter | 0.211 | m |
| Length of stator and rotor cores | 0.185 | m |
| Air gap width | 0.0006 | m |
| Stator back height | 0.01 | m |
| Stator slot height | 0.041 | m |
| Rotor slot height | 0.025 | m |
| Stator slot width (inner/outer) | 3.2/9 | mm |
| Rotor slot width (inner/outer) | 11/8 | mm |
| Number of stator slots | 48 | – |
| Number of rotor slots | 36 | – |
| Number of conductors in one winding | 17 | – |
| Motor efficiency | 91.5 | % |
| Power factor | 0.87 | - |
| Nomber of phases | 3 | - |
| Winding connection | star | - |

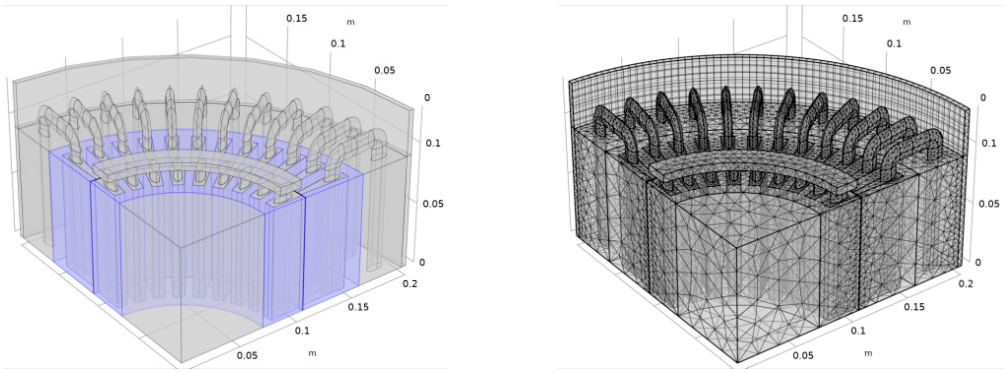

(**a**) (**b**)

**Figure 2.** A computational model of investigated motor: (**a**) geometry; (**b**) mesh.

The mesh has the "swept" distribution type at the outer boundary of the model and in the air gap region (Figure 2a). This is necessary for calculations at the boundary between the moving and stationary parts of the model, which describes the processes in the rotor and stator. A special grid was applied manually to the side boundaries of the model sector in order to ensure its symmetry. Thus, continuity conditions act on the side boundaries, which simulate a "full rendering" of the motor geometry. The features of the simulation model of investigated motor are described in more detail in [26].

## 5. Modeling of Mechano-Acoustic Processes in the Motor Powered by Voltage with Harmonic Distortion

As noted earlier, the main source of SCIM vibration is waves of radial magnetic forces caused by the interaction of the first harmonic of the magnetic field with harmonics of a higher order. Obviously, the vibrations are caused harmonics, which are characterized by a large amplitude and low frequency. The harmonics $g$ = 3, 5, 7, 11, 13 caused vibrations with frequencies $f$ = 400, 600, 800, 1200, 1400 Hz according to Equation (8). These harmonics can be caused by the operation of the inverter and other consumers connected to the network.

It was found in [26] that in the range of 0–2500 Hz, the investigated motor has four modes of natural frequencies: $f_1$ = 165 Hz; $f_2$ = 571 Hz; $f_3$ = 1556 Hz; $f_4$ = 1764 Hz. According to Equation (8), the first two oscillation modes can be enhanced by the interaction of the first harmonic of the magnetic field with the harmonic $g_3 = 3$ at $r = 0$ and with the harmonic $g_5 = 5$ at $r = 4$.

Using the simulation model, studies of the variables characterizing the magnetic noise and vibration of the SCIM stator and torque were carried out. The results of simulation of mechanical stresses in the SCIM stator are shown in Figure 3.

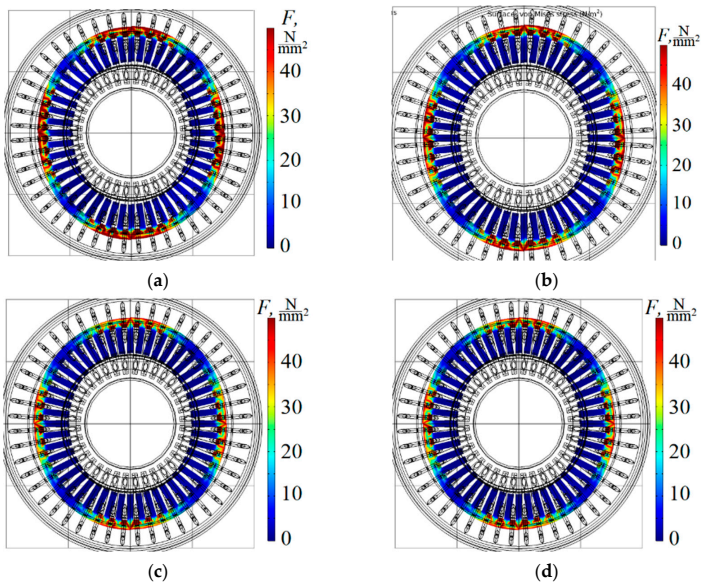


**Figure 3.** Von Mises stress in the stator core of the investigated motor with harmonic distortion of the supply voltage: (**a**) $I_{g3} = I_{g5} = 0$ A; (**b**) $I_{g3}$ = 8.8 A, $I_{g5}$ = 3.3 A; (**c**) $I_{g3}$ = 15.4 A, $I_{g5}$ = 7.7 A; (**d**) $I_{g3}$ = 15.4 A, $I_{g5}$ = 7.7 A, $I_A = 1.4 \cdot I_B = 0.8 \cdot I_C$.

An analysis of the mechanical stresses of the stator showed that the amplitude of mechanical stresses in the stator steel decreases when added with high harmonics. Figure 3d shows a graph of the mechanical stresses of the stator when the shape of the supply voltage is distorted by both higher harmonics and amplitude imbalance (the effect of the phase shift of the supply voltage wave was not considered). A similar situation is observed when considering the graphs of acoustic pressure radiated by the motor stator, as shown in Figure 4. The load torque is 10 Nm (5% of the nominal 195 Nm). The coefficients of the negative and positive sequence components $k_{0u} = k_{2u} = 0\%$ for case $I_{g3} = I_{g5} = 0$ A; $k_{0u} = 7\%$, $k_{2u} = 8\%$ for case $I_{g3}$ = 8.8 A, $I_{g5}$ = 3.3 A and $k_{0u} = 23\%$, $k_{2u} = 18\%$ for case $I_{g3}$ = 15.4 A, $I_{g5}$ = 7.7 A.

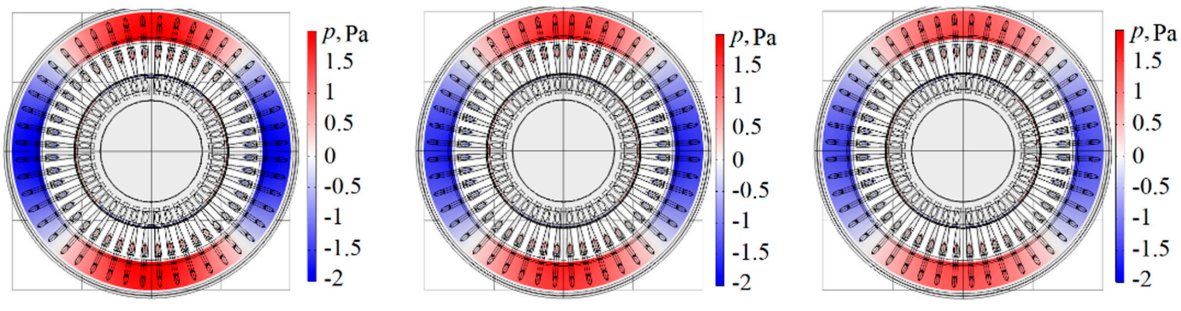


**Figure 4.** Acoustic radiation pressure of investigated motor with harmonic distortion of the supply voltage: (**a**) $I_{g3} = I_{g5} = 0$ A; (**b**) $I_{g3}$ = 8.8 A, $I_{g5}$ = 3.3 A; (**c**) $I_{g3}$ = 15.4 A, $I_{g5}$ = 7.7 A.

According to Figure 4, the acoustic pressure $p$ radiated by the SCIM reaches an amplitude of 2 Pa, which corresponds to a noise level $L_p$ = 100 dB (relative to the reference value of 20 μPa). The expression [29,30] was used in the following calculation:

$$L_p = 20\lg\frac{p}{20 \times 10^{-6}} \quad (10)$$

At the same time, at the stage of frequency analysis, an increase in mechanical deformations caused by the influence of harmonics $g_3$ and $g_5$ was revealed. These graphs are shown in Figure 5.

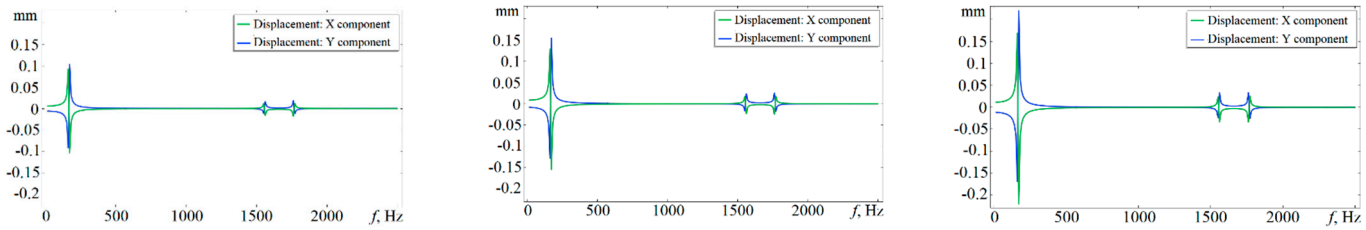


(**a**) (**b**) (**c**)

**Figure 5.** Frequency responses of displacement of the stator of the investigated motor with harmonic distortion of the supply voltage: (**a**) $I_{g3}$ = $I_{g5}$ = 0 A; (**b**) $I_{g3}$ = 8.8 A, $I_{g5}$ = 3.3 A; (**c**) $I_{g3}$ = 15.4 A, $I_{g5}$ = 7.7 A.

According to Figure 5, the vibration displacement of the stator with the square form of the supply increased two-fold at frequencies $f_1$ = 165 Hz and $f_3$ = 1556 Hz and 1.5-fold at $f_4$ = 1764 Hz. Presumably, the sum of the interacted first harmonic of the supply current with the harmonic $g$ = 3 has a lower peak value than the first harmonic itself, which contributed to the reduction in mechanical stress. According to Equation (1), in this case, significantly lower values of radial magnetic forces arise, which act for longer periods and cause greater stator deformations.

Figure 6 shows the time-dependance diagrams of the electromagnetic torque of the investigated motor.

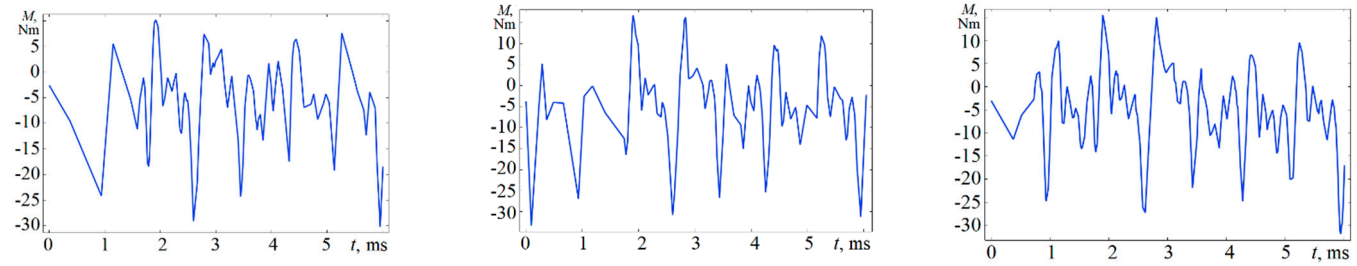


(**a**) (**b**) (**c**)

**Figure 6.** Electromagnetic torque of the investigated motor with harmonic distortion of the supply voltage: (**a**) $I_{g3}$ = $I_{g5}$ = 0 A; (**b**) $I_{g3}$ = 8.8 A, $I_{g5}$ = 3.3 A; (**c**) $I_{g3}$ = 15.4 A, $I_{g5}$ = 7.7 A.

Figure 6 shows curves of the electromagnetic torque for the investigated motor at no load. At the same time, a slight increase in torque ripples can be observed in the case of harmonic distortions of the supply voltage: the range of peak ripple values at $I_{g3}$ = $I_{g5}$ = 0 A was $M_{em}$ = –30 ÷ 9.5 N·m (Figure 6, a), at $I_{g3}$ = 8.8 A, $I_{g5}$ = 3.3 A: $M_{em}$ = –34 ÷ 15.5 N·m (Figure 6, b), at $I_{g3}$ = 15.4 A, $I_{g5}$ = 7.7 A: $M_{em}$ = –31.5 ÷ 14.5 N·m (Figure 6c). This mode can be explained by the interaction of tooth pulsations of the magnetic field with pulsations caused by harmonic distortions.

## 6. Modeling of Mechano-Acoustic Processes in the Motor Powered by Voltage with Amplitude Unbalance

The harmonic composition of the magnetic field waves can be changed in the motor air gap. This may be caused by the supply voltage imbalance. Voltage imbalance studied at the three phase voltages differs only in amplitude. The phase relationship is normal–$2\pi/3$. The results of the simulation of stator mechanical stresses in the case of voltage imbalance are shown in Figure 7.

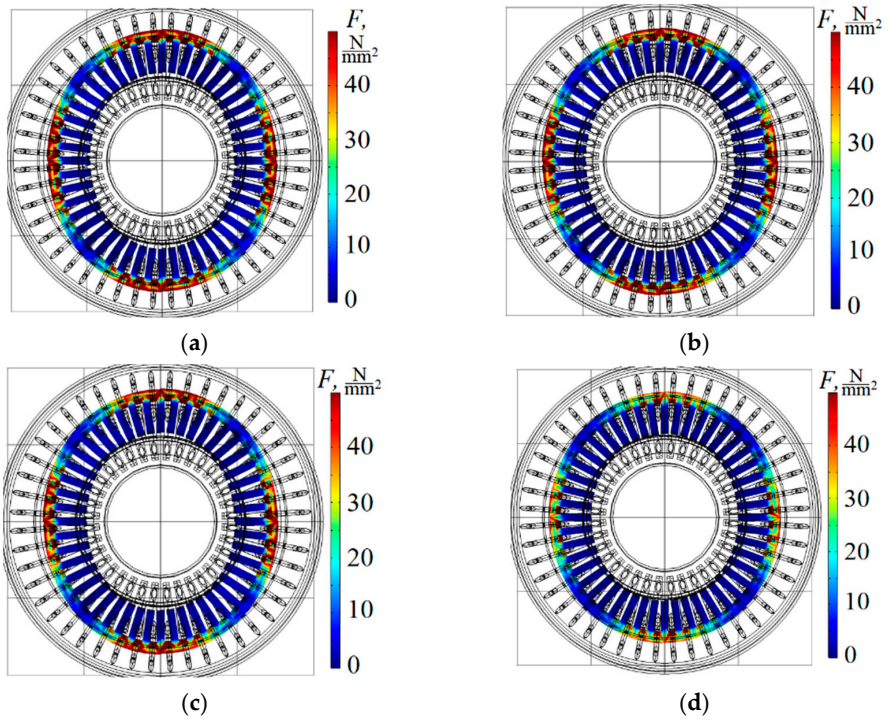


**Figure 7.** Von Mises stress in the stator core of the investigated motor with supply voltage imbalance: (**a**) $I_A = I_B = I_C$; (**b**) $I_A = 1.1 \cdot I_B = 0.9 \cdot I_C$; (**c**) $I_A = 1.4 \cdot I_B = 0.8 \cdot I_C$; (**d**) $I_{g3} = 15.4$ A, $I_{g5} = 7.7$ A, $I_A = 1.4 \cdot I_B = 0.8 \cdot I_C$.

Unlike in the case of harmonic distortions of supply voltages, their amplitude imbalance practically does not affect the value of mechanical stresses caused by the action of radial magnetic forces on the steel core of the stator. A similar situation is observed when analyzing the acoustic pressure graphs shown in Figure 8. The sound pressure at a current asymmetry of ±40% (voltage asymmetry of ±5–8%) is reduced by no more than 20%.

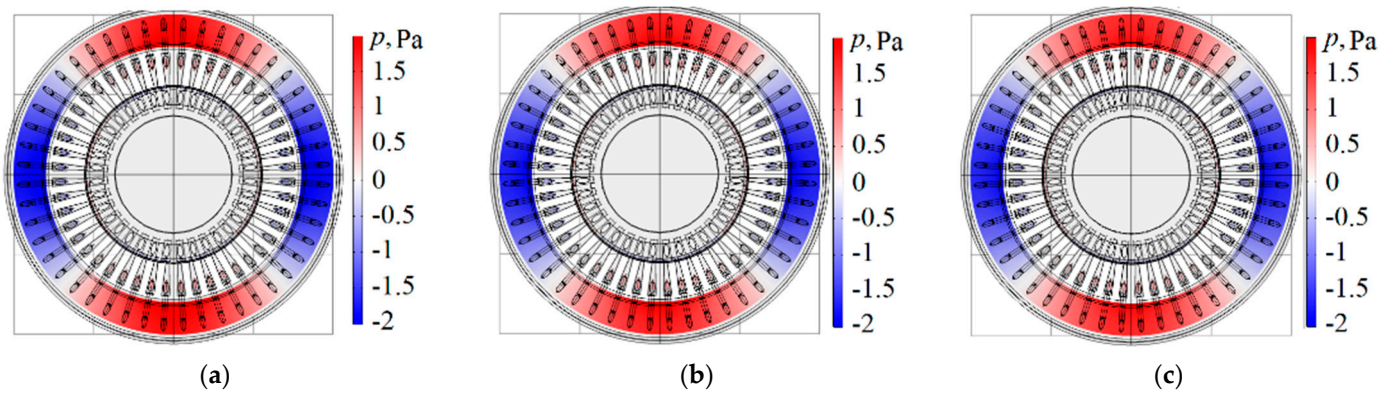


**Figure 8.** Acoustic radiation pressure of the investigated motor with supply voltage imbalance: (**a**) $I_A = I_B = I_C$; (**b**) $I_A = 1.1 \cdot I_B = 0.9 \cdot I_C$; (**c**) $I_A = 1.4 \cdot I_B = 0.8 \cdot I_C$.

Figure 9 shows the frequency responses of the stator vibration displacements caused by the action of radial magnetic forces in the case of amplitude imbalance of the supply voltage.

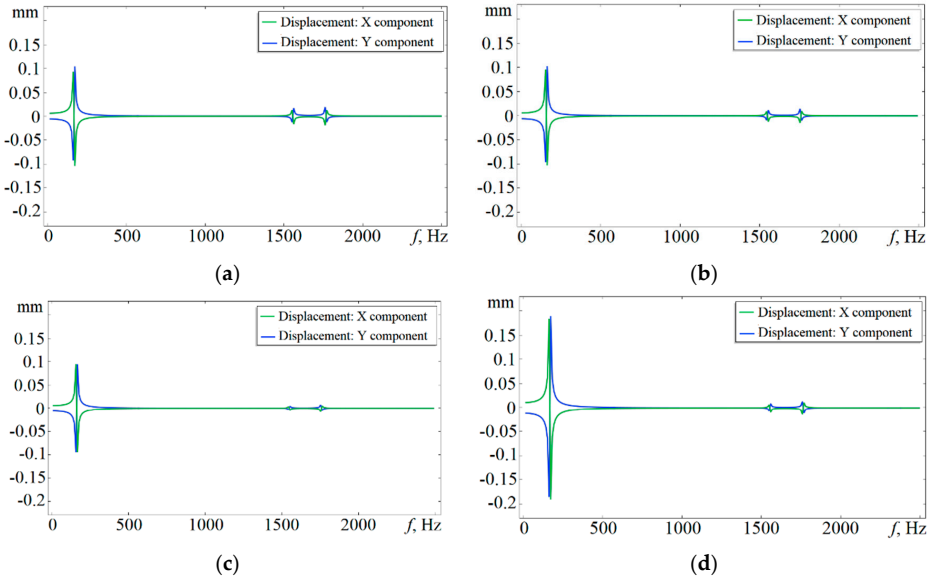


**Figure 9.** Frequency responses of displacement of the stator of the investigated motor with supply voltage imbalance: (**a**) $I_A = I_B = I_C$; (**b**) $I_A = 1.1 \cdot I_B = 0.9 \cdot I_C$; (**c**) $I_A = 1.4 \cdot I_B = 0.8 \cdot I_C$; (**d**) $I_{g3} = 15.4$ A, $I_{g5} = 7.7$ A, $I_A = 1.4 \cdot I_B = 0.8 \cdot I_C$.

The graphs (Figure 9) show multiple decreases in the amplitude of vibration displacement harmonics with frequencies $f_3 = 1556$ Hz and $f_4 = 1764$ Hz, which correspond to the 15th and 17th harmonics of the magnetic field (and supply voltage). Presumably, these harmonics were caused by the interaction of the first harmonic of the magnetic field with the slot harmonics, which explains their sufficient decrease (by 75% for the harmonics with a frequency $f_3 = 1556$ Hz; by 50% for the harmonics with a frequency of $f_4 = 1764$ Hz), with a slight decrease (no more than 15%) of the first harmonic of vibration displacement.

Figure 10 shows the diagrams of the electromagnetic torque of the investigated motor in the case of supply voltage imbalance.

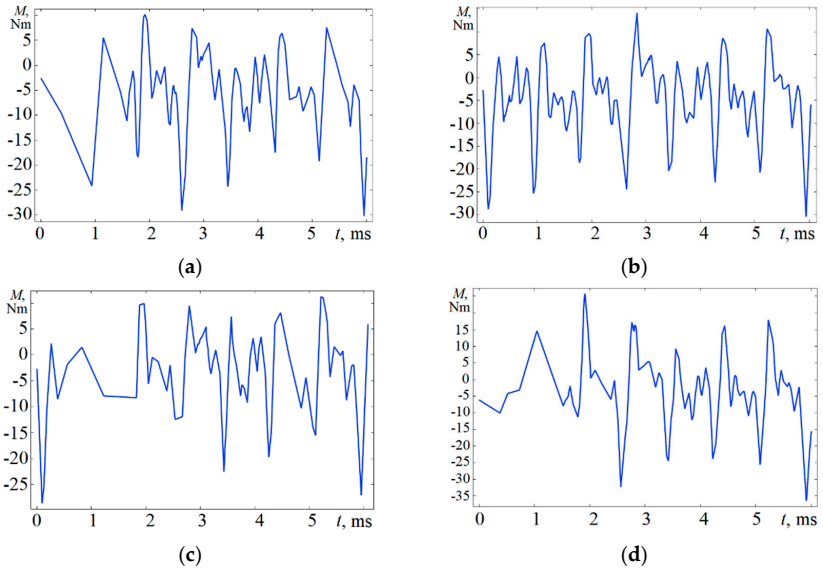


**Figure 10.** Electromagnetic torque of investigated motor with supply voltage imbalance: (**a**) $I_A = I_B = I_C$; (**b**) $I_A = 1.1 \cdot I_B = 0.9 \cdot I_C$; (**c**) $I_A = 1.4 \cdot I_B = 0.8 \cdot I_C$; (**d**) $I_{g3} = 15.4$ A, $I_{g5} = 7.7$ A, $I_A = 1.4 \cdot I_B = 0.8 \cdot I_C$.

It follows from Figure 10 that at currents $I_A$ = 1.1 $I_B$ = 0.9 $I_C$ the torque ripples increased to $M_{em}$ = –30.5 ÷ 13.5 N·m; however, at $I_A$ = 1.4 $I_B$ = 0.8 $I_C$, the torque ripples decreased ($M_{em}$ = −28.5 ÷ 10.5 N·m), which may have been caused by a decrease in the sum of effective current values in the stator windings from 171.0 A to 162.5 A.

## 7. Conclusions

In a multiphysics finite element design software environment, a model allowing study of the electromagnetic, mechano-acoustic and energy processes in a squirrel-cage induction motor was developed. The calculations take into account the interconnectedness and mutual influence of processes occurring at different branches of physics.

It was found that the third and fifth harmonics of the supply voltage have a significant effect on these physical variables, even in the absence of a phase mismatch with the first harmonic of the voltage. In the case of a signal close to the meander ($I_{g1}$ = 57 A, $I_{g3}$ = 15.4 A, $I_{g5}$ = 7.7 A), a decrease in the mechanical stresses of the stator and sound pressure is observed. However, the amplitude of the stator vibration displacements more than doubled. This mechano-acoustic mode is explained by a decrease in the peak value of the supply current due to the superposition of the first and third harmonics and an increase in the duration of the half-wave of the radial magnetic force, which reaches its maximum value faster due to the rectangular shape of the supply voltage.

In the case of the supply voltage imbalance, a significant decrease (by 2–4 times) in the stator vibration disturbances in modes with frequencies $f_3$ = 1556 Hz and $f_4$ = 1764 Hz was observed, presumably caused by the interaction of the first harmonic of the magnetic field with the slot harmonics. In addition, this decrease is aggravated by a decrease in the sum of the effective values of the currents in the SCIM stator windings from 171.0 A to 162.5 A.

The displacements of the stator of the investigated motor were 0.016 mm at the frequency of the fundamental harmonic of the radial magnetic force of 100 Hz. Displacements increased to 0.022 mm (at $I_{g3}$ = 8.8 A, $I_{g5}$ = 3.3 A) and up to 0.027 mm (at $I_{g3}$ = 15.4 A, $I_{g5}$ = 7.7 A) when the supply voltage was distorted by higher harmonics. Voltage imbalance had practically no effect on the motor vibration.

In the future, we plan to use the developed simulation model to further study the effect of the harmonic composition of the supply current and the parameters of its imbalance (phase and amplitude) on the processes of magnetic vibration excitation in the SCIM stators.

**Author Contributions:** Conceptualization, V.E. and A.E.; methodology, A.P.; software, A.E.; validation, A.E. and D.T.; formal analysis, V.E.; investigation, A.E.; resources, D.T.; data curation, A.E.; writing—original draft preparation, A.E.; writing—review and editing, D.T.; visualization, A.E.; supervision, V.E.; project administration, D.T.; funding acquisition, D.T. All authors have read and agreed to the published version of the manuscript.

**Funding:** The work was founded by the Russian Science Foundation (project no. 22-29-01142).

**Data Availability Statement:** No applicable.

**Conflicts of Interest:** The authors declare no conflict of interest.

## Abbreviation

SCIM Squirrel-cage induction motors

## References

1. Xu, X.; Han, Q.; Chu, F. Review of Electromagnetic Vibration in Electrical Machines. *Energies* **2018**, *11*, 1779. [CrossRef]
2. Frosini, L. Novel Diagnostic Techniques for Rotating Electrical Machines—A Review. *Energies* **2020**, *13*, 5066. [CrossRef]
3. Xie, Y.; Chen, P.; Li, F.; Liu, H. Electromagnetic Forces Signature and Vibration Characteristic for Diagnosis Broken Bars In Squirrel Cage Induction Motors. *Mech. Syst. Signal Process.* **2019**, *123*, 554–572. [CrossRef]
4. Maliti, K.C. *Modelling and Analysis of Magnetic Noise in Squirrel-Cage Induction Motors*; Tekniska högsk.: Stockholm, Sweden, 2000.
5. Spagnol, M.; Bregant, L.; Boscarol, A. Electrical Induction Motor Higher Harmonics Analysis Based On Instantaneous Angular Speed Measurement. *Appl. Cond. Mon.* **2016**, *4*, 27–41. [CrossRef]

6. Silwal, B.; Rasilo, P.; Belahcen, A.; Arkkio, A. Influence of the Rotor Eccentricity on the Torque of a Cage Induction Machine. *Arch. Electr. Eng.* **2017**, *66*, 383–396. [CrossRef]
7. Qiu, H.; Yu, W.; Li, Y.; Yang, C. Research On The Influence Of Driving Harmonic On Electromagnetic Field And Temperature Field Of Permanent Magnet Synchronous Motor. *Arch. Electr. Eng.* **2017**, *66*, 295–312. [CrossRef]
8. Zhang, A.; Bai, Y.; Yang, B.; Li, H. Analysis of Nonlinear Vibration in Permanent Magnet Synchronous Motors under Unbalanced Magnetic Pull. *Appl. Sci.* **2018**, *8*, 113. [CrossRef]
9. Ma, C.-G.; Zuo, S.-G.; Sun, Q.; Meng, S. Order Feature Analysis of Electromagnetic Noise in a Permanent Magnet Synchronous Motor Considering Current Harmonics. *Zhendong Yu Chongji/J. Vib.* **2014**, *33*, 108–113. [CrossRef]
10. Senousy, M.; Larsen, P.; Ding, P. Electromagnetics, Structural Harmonics and Acoustics Coupled Simulation on the Stator of an Electric Motor. *SAE Int. J. Passeng. Cars–Mech. Syst.* **2014**, *7*, 822–828. [CrossRef]
11. Sinervo, A.; Arkkio, A. Rotor Radial Position Control and its Effect on the Total Efficiency of a Bearingless Induction Motor with a Cage Rotor. *IEEE Trans. Magn.* **2014**, *50*, 6665149. [CrossRef]
12. Boguslawsky, I.; Korovkin, N.; Hayakawa, M. *Large A.C. Machines: Theory and Investigation Methods of Currents and Losses in Stator and Rotor Meshes Including Operation with Nonlinear Loads*; Springer Nature: Tokyo, Japan, 2016. [CrossRef]
13. Guo, D.; Chu, F.; Chen, D. The Unbalanced Magnetic Pull and Its Effects on Vibration in a Three-Phase Generator with Eccentric Rotor. *J. Sound Vib.* **2002**, *254*, 297–312. [CrossRef]
14. Ruf, A.; Schroder, M.; Putri, A.; Franck, D.; Hameyer, K. Analysis and determination of mechanical bearing load caused by unbalanced magnetic pull. In Proceedings of the 17th International Conference on Electrical Machines and Systems, Hangzhou, China, 22–25 October 2014; pp. 8–14. [CrossRef]
15. Wang, Y.; Li, P.; Ren, G. Electric Vehicles with In-Wheel Switched Reluctance Motors: Coupling Effects between Road Excitation And The Unbalanced Radial Force. *J. Sound Vib.* **2016**, *372*, 69–81. [CrossRef]
16. Ibrahim, I.; Mohammadi, M.H.; Ghorbanian, V.; Lowther, D.A. Effect of Pulsewidth Modulation on Electromagnetic Noise of Interior Permanent Magnet Synchronous Motor Drives. *IEEE Trans. Magn.* **2019**, *55*, 8740965. [CrossRef]
17. Zappala, D.; Sarma, N.; Djurovic, S.; Crabtree, C.J.; Mohammad, A.; Tavner, P.J. Electrical & Mechanical Diagnostic Indicators Of Wind Turbine Induction Generator Rotor Faults. *Renew. Energy* **2019**, *131*, 14–24. [CrossRef]
18. Kirschneck, M.; Rixen, D.J.; Polinder, H.; Van Ostayen, R.A.J. Electromagnetomechanical Coupled Vibration Analysis of a Direct-Drive Off-Shore Wind Turbine Generator. *J. Comput. Nonlinear Dyn.* **2015**, *10*, 041011. [CrossRef]
19. Astakhov, N.V.; Malyshev, V.S. Calculating the Air-Gap Permeance of Induction Motors In the Presence of Eccentricity. *Sov. Electr. Eng.* **1980**, *51*, 34–38.
20. Shubov, I.G. *Noise and Vibration of Electrical Machines*, 2nd ed.; Energoatomizdat: Leningrad, Russia, 1986.
21. Cassoret, B.; Corton, R.; Roger, D.; Brudny, J.-F. Magnetic Noise Reduction of Induction Machines. *IEEE Trans. Power Electron.* **2003**, *18*, 570–579. [CrossRef]
22. Pellerey, P.; Favennec, G.; Lanfranchi, V.; Friedrich, G. Active Reduction of Electrical Machines Magnetic Noise by the Control of Low Frequency Current Harmonics. In Proceedings of the 38th Annual Conference on IEEE Industrial Electronics Society, Montreal, QC, Canada, 25–28 October 2012; pp. 1654–1659. [CrossRef]
23. Leleu, E.; Espanet, C.; Miraoui, A.; Siala, S. Analytical Modelling Of Electromagnetic Origin Vibrations In An Induction Machine Supplied By High Power PWM Inverter. In Proceedings of the 32nd Annual Conference on IEEE Industrial Electronics, Paris, France, 6–10 November 2006; pp. 836–843. [CrossRef]
24. Binojkumar, A.C.; Saritha, B.; Narayanan, G. Acoustic Noise Characterization of Space-Vector Modulated Induction Motor Drives—An Experimental Approach. *IEEE Trans. Ind. Electron.* **2015**, *62*, 3362–3371. [CrossRef]
25. Franck, D.; Giet, M.; Hameyer, K. Active Reduction of Audible Noise Exciting Radial Force-Density Waves in Induction Motors. In Proceedings of the IEEE International Electric Machines & Drives Conference, Niagara Falls, ON, Canada, 15–18 May 2011; pp. 1213–1218. [CrossRef]
26. Ermolaev, A.; Erofeev, V.; Plekhov, A.; Titov, D. Active Reduction Of Magnetic Noise Occurring in the Stators of An Induction Motors. *Vibroeng. Procedia* **2021**, *38*, 172–178. [CrossRef]
27. Ermolaev, A.I.; Erofeev, V.I.; Plekhov, A.S.; Titov, D.Y. Study of magnetic vibration occurring in induction motor using FEM simulation. *Smart Electr. Eng.* **2021**, *3*, 37–56. [CrossRef]
28. Shahaj, A. Mitigation of Vibration in Large Electrical Machines. Ph.D. Thesis, University of Nottingham, Nottingham, UK, 2010.
29. Sathyan, S.; Aydin, U.; Belahcen, A. Acoustic Noise Computation of Electrical Motors Using the Boundary Element Method. *Energies* **2020**, *13*, 245. [CrossRef]
30. Nau, S.; Mello, H. Acoustic Noise in Induction Motors: Causes and Solutions. In Proceedings of the Annual Petroleum and Chemical Industry Conference, San Antonio, TX, USA, 13 September 2000; pp. 253–263. [CrossRef]